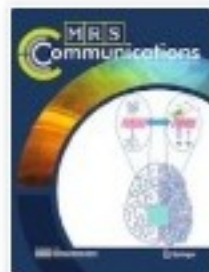





MRS Communications

[Journal home](#) > [Volumes and issues](#) > Volume 12, issue 4

Search within journal



Volume 12, issue 4, August 2022

11 articles in this issue



Experimental validation on multi-pass weld distortion behavior of structural offshore steel HSLA S460 using FE-based inherent strain and thermo-mechanical method

Y. O. Busari^{ID}, Smart Manufacturing Research Institute and School of Mechanical Engineering, Universiti Teknologi MARA (UiTM) Shah Alam, Shah Alam, Malaysia; Department of Materials & Metallurgical Engineering, University of Ilorin, Ilorin, Nigeria

Y. H. P. Manurung, Smart Manufacturing Research Institute and School of Mechanical Engineering, Universiti Teknologi MARA (UiTM) Shah Alam, Shah Alam, Malaysia

Y. L. Shuaib-Babata, Department of Materials & Metallurgical Engineering, University of Ilorin, Ilorin, Nigeria

S. N. Ahmad, and **T. Taufek**, Smart Manufacturing Research Institute and School of Mechanical Engineering, Universiti Teknologi MARA (UiTM) Shah Alam, Shah Alam, Malaysia

M. Leitner, Institute of Structural Durability and Railway Technology, Graz University of Technology, Graz, Austria

J. R. C. Dizon, Design, Research, Extension in Additive Manufacturing, Advanced Manufacturing (DR3AM) Center, Bataan Peninsula State University, City of Balanga, Philippines

N. Muhammad, Jabatan Kejuruteraan Mekanikal, Politeknik Sultan Salahuddin Abdul Aziz Shah, Shah Alam, Malaysia

M. A. Mohamed, Serba Dinamik Group Berhad, Shah Alam, Malaysia

Address all correspondence to Y. H. P. Manurung at yupiter.manurung@uitm.edu.my

(Received 18 October 2021; accepted 9 December 2021; published online: 29 January 2022)

Abstract

This study focuses on prediction of distortion behavior of multi-pass GMAW of structural offshore steel S460G2 + M using thermo-mechanical (TMM) and inherent strain (ISM) methods. In TMM, material properties including plasticity model were obtained from advanced material modeling software based on characterized elemental compositions and double ellipsoid heat source model is implemented. In ISM, residual plastic strain theory is developed based on initial strain value calculated in longitudinal and transverse direction. The predicted distortion and experiment values show an error margin within the range of 8% using TMM and 12% applying ISM with very low computation time.

Introduction

High strength low alloy steel (HSLA) are generally micro alloyed elements when produced through thermo-mechanical controlled process (TMCP) is considered to have increased strength and toughness with low carbon equivalent and excellent weldability. This reduces the pre-heating requirements and susceptibility to cold cracking.^[1, 2] However, the strength and premature failure of welded structural steels has been greatly examined recently which describes the influence of thermal, distortion and residual stress as a major factor that affects the fatigue strength.^[3] This is still a problem despite vast research efforts to alleviate these problems with the geometry design, heat input and material thickness. The challenge of the multi-pass welding process is the difference in the heat input of the same weld line in a structural component, Terasaki et al. noted that the maximal heat input during multi-pass welding determines the inherent strain distribution.^[4]

Welding procedure is vital in steel construction and manufacturing processes due to its accessibility and economy, particularly the gas metal arc welding (GMAW). However, the thermal differential in weld, base metal and the surrounding

as the weld joint cools to maintain a bond with the shrinking weld material in both longitudinal and transverse directions usually result in residual stresses and weld deformation. This is caused mainly by the longitudinal and transverse inherent strain at the weld and its vicinity.^[5] Mitigating distortion obviously increases the welding residual stress and the measurement of such stress is mostly destructive, semi-destructive and non-destructive poses some limitation depending on the area of weld and application. Therefore, Finite element numerical prediction methods have become an important tool in welding, which enables effective planning and decreases the cost of optimization of welding variables by the reduction of exploratory tests before the actual welding.^[6, 7]

Nevertheless, the ability to accurately predict the anticipated weld distortion in mechanical assemblies is crucial in welding simulations. The deformation effect of inherent strain is vital because the deformation and the residual stress produced during welding are caused by the irreversible strain or the inherent strain formed in the plastic deformation process.^[8] Evaluation of weld deformation entails experimental solution based on the elastic theory of applied strain to the pre-weld state analytically, FEM based thermal elastic–plastic method and FEM inherent

strain.^[9, 10] Many works of literature reported the proposed experimental-based inherent strain or equivalent load method. The proposed model derives a moment equation which yields very similar angular deformation according to experimental estimation.^[11] The great feature of the ISM is that only elastic analysis is needed in the FEM to predict welding distortion. Jang et al. (2007) utilize FEM to describe the weld deformation in steel with elastic equivalent force obtained from the analysis at the irreversible region of heat affected zone (HAZ).^[12] Ha and Choi (2015), proposed a modified integration of temperature difference for strain-boundary method in multi-pass weld by considering the contribution of each weld layer to the whole weldment, to represent the curve distortion increment and cumulative distortion.^[13] The application of inherent strain database by Okano et al. (2016) for simplified distortion analysis considered the residual stress effect on the existing weld bead to enhance the accuracy in a multi-pass welding deformation analysis.^[14]

Furthermore, Satoshi et al. (2019) gave an insight on the inherent strain theory as dependent on the value of the second moment of area and radius of induced inherent strain within the mechanical melting zone and the weld length for welding deformation.^[15] The application of inherent strains as a structural boundary condition, combined the effect of plastic, thermal, creep and phase transformation strains in the simulation process. All the elements in the HAZ are assigned with the user pre-determined inherent strains of the effective area or the welding kinematics where integration points falling inside the moving weld pool dimensions are assigned inherent strains.^[16] Commercial software presents a reasonably accurate alternative to predict distortion and residual stress in welding simulation.

Over the years, thermo-mechanical numerical methods have predicted and quantified the effect of the distortion and residual stress during the welding process remarkably well. Model size often determines the computational cost and time. A typical simulation of FEM thermo-elastic-plastic welding distortion undergoes a transient process of thermal then structural analysis with constraints. However, the computational time for thermo-mechanical analysis of multi-pass welding is enormous. Usually, the decision of balanced trade-off between model size and extent of details in simulation is made, particularly with the thermo-mechanical behavior in many welding simulations.

Based on the reviewed literature, few numerical investigations emphasized on the weld distortion of HSLA steel such as S460 using inherent strain method and thermo-mechanical methods for material data developed from thermodynamic and property databases program, utilized for plasticity model and heat transfer coefficients where the thermal distribution within weld pool is adjusted. For these reasons, this study analyses the three-layer Butt-joint with GMAW using the computational approaches of ISM-User Defined and non-linear TMM provided in MSC Marc/Mentat which will be compared to experimental results. Hence, the

ultimate purposes are to examine the effect of the process parameters and actual material utilized in the experiment and to estimate the overall welding distortion behavior of this steel. The analysis began with modification of heat source and transfer coefficient and comparing the experimental and simulated transient thermal curves at different locations. It is expected that the potential capability of the prediction method with respect to computational time for three-layer welded butt-joint is demonstrated.

Numerical computation using thermo-mechanical and inherent strain method

The FE analysis to predict the mechanical properties by variation of several parameters to ensure prior alleviation measures to enhance and compliment a sound weld from conventional experimental approach, can be tackled using the current computational approach. However, the computational resources and time further complicate this process, particularly weld deformation in HSLA steel structures due to the material phase changes during heating, melting, and solidification during welding since comprehensive techniques to simulate the multi-disciplinary physics of welding are still evolving. Therefore, the use of the elastic-plastic FE methods for solid bodies is a valuable method for welding simulations where the inherent strain value is assessed empirically for the process variables, physical properties in the effective area of the weld region and heat affected zone. Both 3D numerical analysis is developed using FE software MSC Marc/Mentat to predict the welding process of HSLA S460 steel.

Geometrical modeling of butt-joint

The three-dimensional FEM model with three-layer butt-joint welding using MSC Marc/Mentat computational software, with each zone discretized using quad elements, and with finer mesh at the weld region as seen in Fig. 1(a) with hexahedral meshing. However, thermal and structural boundary conditions engaged in the FEM analysis distinguish non-linear thermo-mechanical analysis and ISM of user-defined parameters. The model consists of 6109 total nodes with 4,848 solid elements, and two individual parts with the same dimension of 100 mm × 150 mm × 10 mm. the weld zone is assumed to encroach into the base plate, the adjacent layer of elements to the weld bead is assigned weld metal yield properties to avoid strain history errors associated with parent material melting.

Welding simulation using TMM

This process of welding computational implements sequential evaluation of the thermal and structural fields within the same finite element mesh. The results on the effect of thermal analysis serves as the input for the next structural analysis. The thermo-mechanical computational multi-pass welding analysis using FEM requires an

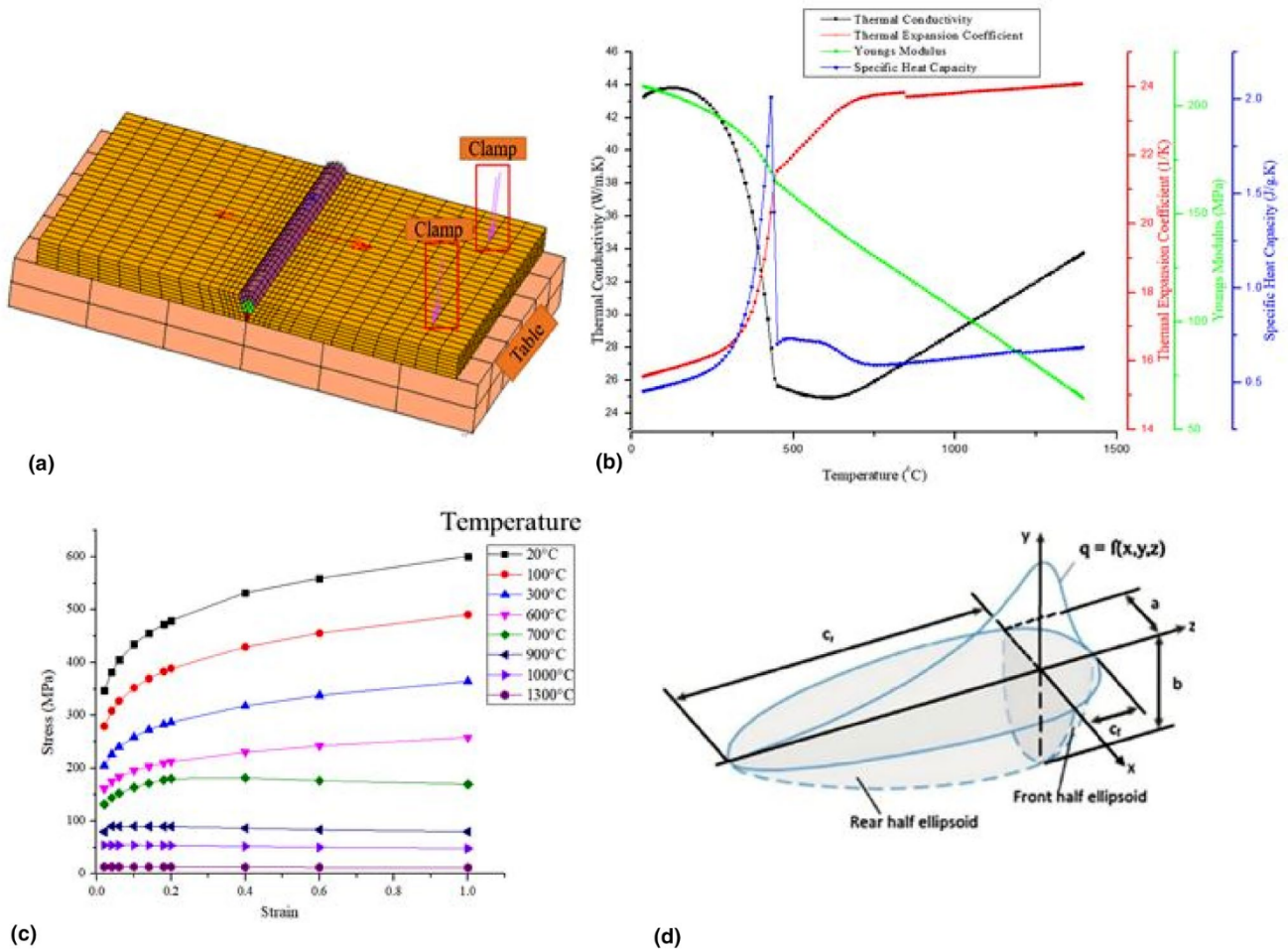


Figure 1. (a) Finite element models, S460 material data (b) Temperature-dependent mechanical and thermophysical (c) Flow curve at strain rate 0.01 s^{-1} , (d) Goldak's double ellipsoidal heat source model.

appropriate form of transient thermal model. The timing of distribution of heat source surface and volume are defined based on the welding condition, which is adequately calibrated together with the temperature-dependent material properties. Metal vaporization, however, is neglected. It is assumed that the effect of vaporization is included in the arc efficiency parameter.^[17] The heat conduction governing equation in solid is defined as Eq. (1):

$$\frac{\partial}{\partial x} \left(K \frac{\partial T}{\partial x} \right) + \frac{\partial}{\partial y} \left(K \frac{\partial T}{\partial y} \right) + \frac{\partial}{\partial z} \left(K \frac{\partial T}{\partial z} \right) = \rho C \frac{\partial T}{\partial t} \quad (1)$$

where the weld-piece is defined with density (ρ), temperature (T), specific heat (C) and time (t) respectively. Thermal conductivity (k) describes the associated boundary condition towards ambient temperature. TMM modeling is used to demonstrate the effects of heating on the re-solidified welded plate with the calculation of energy balance in Eq. (2). Q is the volumetric heat rate; ∇ is the Laplace operator; The heat flux (q) is defined for heat conduction, convection and radiation and their heat transfer coefficient equations are applied to all relevant surfaces and the weld bead surface and no creep effect was considered.

$$\rho C \frac{\partial T}{\partial t} + \nabla \cdot q - Q = 0 \quad (2)$$

The conduction heat flux for thermal conductivity (k) of the material describing associated boundary condition in this work towards the ambient temperature is describe in Eq. (3)

$$q_{\text{Conduction}} = -k \nabla T \quad (3)$$

Furthermore, during the arc welding process, heat dissipated to the environment by convection is described in Eq. (4). Where H_c is convective heat transfer coefficient to the surrounding, T_w is the weld pool temperature and T_o is the ambient temperature.

$$q_{\text{Convection}} = H_c (T_w - T_o) \quad (4)$$

The heat flux losses from the welded plate surface due to radiation is defined in the linearize Eq. (5), where ε is the emissivity and σ is the Stefan-Boltzman constant.

$$q_{\text{Radiation}} = \varepsilon \sigma (T_w^4 - T_o^4) \quad (5)$$

The mechanical analysis is implemented in the FEM procedures subsequently after thermal simulation of temperature

history for each nodes in the mesh. The time steps in the thermal and mechanics problem are independent of each other and in fact different time steps may be required to ensure convergence. The system of equilibrium equations is solved in a series of small increments. The quasi-static balance of momentum is determined for each step using Eq. (6).

$$\nabla \cdot \sigma + \rho f = 0 \quad (6)$$

where f is the body force per unit mass and the displacement vector variable is required for constitutive relation of stress, strain and material kinematic. Furthermore, consequences of a thermal analysis and the incremental and total strain for the purpose of numerical realization of welding simulation is modeled with isotropic hardening rule. The yield surface expands with accumulated plastic strain.^[18] The yielding occurs with the implementation of plastic incompressibility, initial isotropy, isotropic hardening and the normality rule are defined in Eq. (7).

$$f = \sigma_{eq} - H - \sigma_y \quad (7)$$

where σ_{eq} is the von mises equivalent stress, σ_y is the initial yield stress and H is the degree of strain hardening as the values of flow stress would decrease with the elevation of temperature as depicted in Fig. 1(c) of the stress–strain curve.

Temperature-dependent material properties and modeling

The HSLA sheet and filler wire that conforms with AWS A5.28/A5.28M: 2005 material composition performed with optical emission spectrometry analysis in Table I. The composition for both the HSLA 460 steel and Filler metal ER80S-Ni1 is used to generate thermal expansion coefficient, thermal conductivity, modulus of elasticity, specific heat capacity and the flow curve using JMatPro software, which was calculated by means of all thermodynamics and physical properties by Calculation of

Phase Diagrams method which was based on an equilibrium of phase diagram. The physical properties are mostly influenced by the chemical composition thus it is possible to be calculated by first assessing the chemical composition as the input for the JMATPRO calculation.^[19, 20] The characterization of the plastic behavior, flow stresses were modeled using the isotropic hardening rule and Von Mises yield criterion for base and filler metal. Furthermore, the temperature-dependent thermophysical properties of material S460 is described in Fig. 1(b). The relationship between flow stress and plastic strain of both the base metal at strain rates of 0.001 s⁻¹ is depicted in Fig. 1(c). The plasticity model according to isotropic hardening rule using Von Mises yield criteria with strain rate 0.01 s⁻¹ for S460.

Heat source modeling and calibration

The volumetric moving double ellipsoidal heat source model, as seen in Fig. 1(d) from Goldak et al. has proven to be very effective for a wide range of arc welding techniques.

The fraction of deposited head F_f and F_r represents the heat apportionments of the heat flux in the front and rear quadrants, provided that the condition $F_f + F_r = 2$ is fulfilled. The fractions can be assumed as $f_f = \frac{2C_f}{C_f + C_r}$ and $f_r = \frac{2C_r}{C_f + C_r}$ if the volumetric heat source is considered. Furthermore, the method defines a volume of material as the weld pool and weld heat flux, which navigate the model along the weld groove, and relates subsequently with active element to simulate the weld metal is governed by Goldak and Akhlaghi^[21] Eq. (8).

$$q_{vf/r}(x, y, z) = \frac{6\sqrt{3}f_{f/r}Q}{abc_{f/r}\pi\sqrt{\pi}} e^{-3\frac{x^2}{a^2}} \cdot e^{-3\frac{y^2}{b^2}} \cdot e^{-3\frac{z^2}{c_{f/r}^2}} \quad (8)$$

Width (a), depth (b), rear length (c_r) and front length (c_f) describe the direction of the heat flux distribution in the double ellipsoid model. The heat flux in the front and rear quadrant were the fractions of heat deposited, provide that the condition

Table I. Chemical composition and welding parameter.

Elements	C	Si	Mn	P	Cr	Ni	Cu	Al	S	Fe
<i>HSLA S460 steel</i>										
Wt (%)	0.088	0.429	1.50	0.015	0.047	0.033	0.041	0.03	<0.0005	Bal
<i>Filler wire ER 80S-Ni1</i>										
Elements	C		Ni	Mn	Cu	Mo	P	Si	S	Fe
Wt (%)	0.10		1.0	1.10	0.12	0.10	0.01	0.01	0.01	Bal
Heat source dimension and weld parameters										
Heat source dimensions	First pass			Second pass			Capping			
Width (a) (mm)	3.5			5			6.5			
Depth (b) (mm)	4.5			4			4			
Forward length (C_f) (mm)	4.5			4			5.5			
Rear length (C_r) (mm)	13.5			11			16.5			
Current (A)	83			136			140			
Voltage (V)	22			22			21			
Travel speed (mm/s)	6			6.5			3.5			

$f_f + f_r = 2$. The values for each direction employed in each layer of the boundary conditions for FEM welding simulation and parameters are shown in Table I. The thermal boundary condition assigned in the FEM simulation were Latent heat ($2.564 \times 10^{11} \text{ mm/s}^2$), solidus (1309°C) and liquidus (1452°C) temperatures based on the real thermal properties of S460 material data investigated in the software program section. The heat model efficiency was taken as 0.8.

In Fig. 2(b), the reference region shows a simulated HAZ scale (width) compared to the empirically measured HAZ size in the relevant regions obtained from the etched macrostructure in the right-side image. This heat conduction surface was designed uniquely for each weld layer based on the geometry of the newly deposited weld metal. Moreover, the constituent of fusion zone and penetration profile isothermal contour plots display excellent match with the weld passes macrographs observed under optical micrograph of $\times 5$ magnification.

Heat source calibration is essential for thermo elastic plastic welding simulation to ensure the neglected influence shield in gas, active elements, flowing weld bath and so on. The transient temperature distribution is employed as the calibration method in this study during actual multi-pass welding process and similar position in the simulation illustrated in Fig. 2(a).

In Fig. 2(d–f), the measured thermal cycle histories with type-K thermocouple of 1.2 mm diameter in the experiment and corresponding node in the FEM simulation display good conformity at 5 mm (node 16,366), 10 mm (node 16,573) and 15 mm (node 20,212) distance to the weld groove. The ultimate temperatures in the simulation for three passes are slightly lower than those measured. For heat effect consideration of the weld specimen to the welding table and the environment, Heat Transfer Coefficient, metal to metal of $2500 \text{ W/m}^2/^\circ\text{C}$ and metal to the environment of $25 \text{ W/m}^2/^\circ\text{C}$ were applied. The initial temperature was set at 34°C according to the measurements. The thermal conductivity was synthetically increased to compensate

for the effect of convection heat transfer due to blending in the molten weld pool.

Welding simulation using user-defined Inherent Strain Method (ISM-UD)

This method in welding deformation estimates the inherent strain value considering the maximum temperature, temperature gradient in the vertical direction of welding line, and the size of the heat affected zone. The temperature loading method is developed to load the variable inherent strain value expediently.

Principle of ISM

This first section covers the mechanism of the empirical formula governing inherent strain. Distortion in a welded component emanates from the huge temperature variance between the molten weld pool and the adjacent base material resulting in internal stresses or total residual strain in an attempt to stabilize the temperature differences in the weld metal regions. The total strain (ε) can be broken down into thermal strain (ε_T), elastic strain (ε_e), plastic strain (ε_p), creep strain (ε_c) and the strain developed with phase transformation (ε_{PT}). Deng et al. described the total strain increment in Eq. (9) based on mechanical analysis.^[22]

$$\varepsilon = \Delta\varepsilon_e + \Delta\varepsilon_p + \Delta\varepsilon_T + \Delta\varepsilon_c + \Delta\varepsilon_{PT} \quad (9)$$

When the welded specimen has fully cooled-off, the creep strain becomes insignificant. For mild steel, phase transformation has an insignificant effect on the welding deformation.^[9] Also, the thermal strain becomes zero. Therefore, Eq. (10) sums the total strain as;

$$\varepsilon = \Delta\varepsilon_e + \Delta\varepsilon_p \quad (10)$$

The inherent strain (ε^*) is defined by the difference between Plastic strain and elastic strain written in Eq. (11)^[23] as:

$$\varepsilon^* = \varepsilon_p - \varepsilon_e \quad (11)$$

Furthermore, Eq. (11) can be rearranged to become Eq. (12)

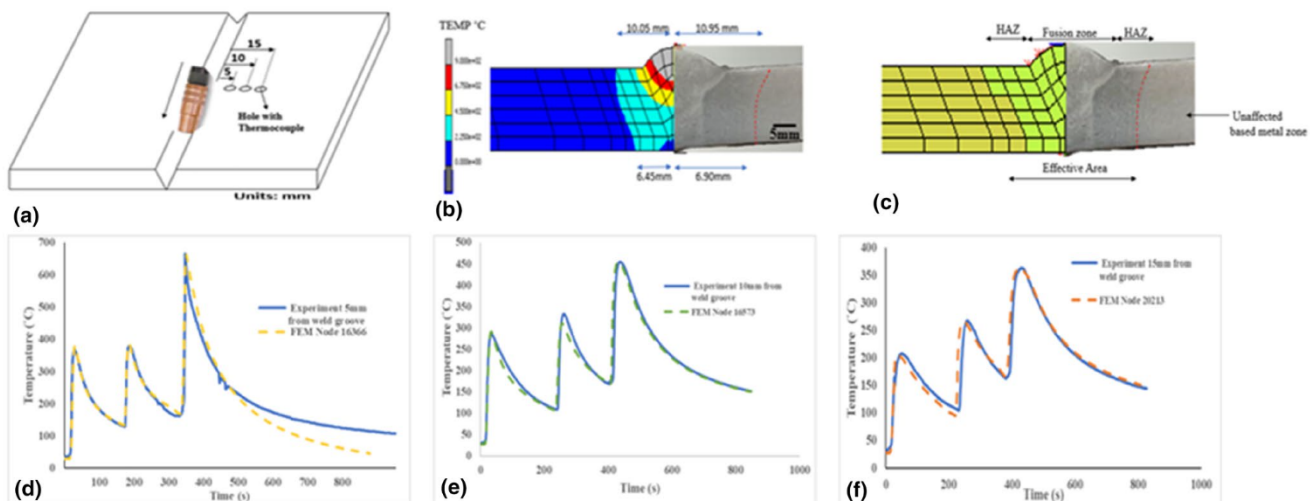


Figure 2. (a) Thermocouple wire location and equivalent position in the FEM. (b) Calibration of macrograph and isotherms for the weld. (c) Symmetrical representation of the effective areas with Macro-etched weld specimen. FEM simulation calibration at (d) Point 1 (e) Point 2 (f) Point 3.

$$\varepsilon_p = \varepsilon - \Delta\varepsilon_e \quad (12)$$

Hence, the inherent strain is the same as the plastic strain at the end of the cooling process^[24, 25] as depicted in Eq. (13)

$$\varepsilon^* = \varepsilon - \Delta\varepsilon_e + \varepsilon_p \quad (13)$$

However, Inherent strains exhibit different behaviors with respect to maximum temperatures within the weld zone. Therefore, at the end of each of the thermal cycles, the compressive plastic strains (plastic strain zone) in the weld zone and its adjacent surrounding area remains the same as the amount of inherent strain ε^* in the welding process.^[26, 27] Substituting the total strain in Eq. (13) yields Eq. (14).

$$\varepsilon^* = \Delta\varepsilon_p + \Delta\varepsilon_T + \Delta\varepsilon_{Pl} \quad (14)$$

Jang et al. proposed a disk-spring model that used the strain-based equivalent load method to analyze three-dimensional structures.^[28] Kim et al. also calculated an inherent strain considering the temperature.^[29] Furthermore, Luo et al. proposed an inherent strain production under three-dimensional FEM constraints for plane strain model with the influence of the highest temperature in the welding direction at steady-state temperature in Eq. (15).

$$\varepsilon^* = -\varepsilon_x^* = 0 \quad (15)$$

And Eq. (16) at elevated temperature

$$\varepsilon^* = -\varepsilon_x^* = -\alpha (\Delta T) \quad (16)$$

Therefore, the inherent strain becomes Eq. (17).

$$\varepsilon^* = -\varepsilon_x^* \quad (17)$$

In inherent strain estimation, the equivalent strain and equivalent load method are the same in simple structures.^[10] In FE analysis, the inherent strain value to the effective area is calculated relative to the strains involved in the heat transfer analysis as proposed by Kim et al.^[24]

In this study, the stiffness was on one side of the welded specimen, the longitudinal inherent strain and transverse inherent strain were considered for each weld and the position where strains exist, with the thermal load of units which can be obtained by elastic FEM analysis weld deformation. Hence, the total inherent strain in welding process was defined in Eq. (18) as follows:

$$\varepsilon = -W/A \quad (18)$$

The summation of the longitudinal inherent strain ε_x^* and transverse inherent strain ε_y^* in the unit length were W_x and W_y and its relationship with the heat input Q in the welding process was expressed as Eqs. (19) and (20) respectively:

$$W_x = KQ \quad (19)$$

$$W_y = \xi Q \quad (20)$$

where K and ξ in Eqs. (21) and (22) were the thickness coefficients as proposed by Ueda et al.

$$K = (0.255 - 0.335)\alpha/C\rho \quad (21)$$

$$\xi = (0.255 - 1.0)\alpha/C\rho \quad (22)$$

where α was the thermal expansion coefficient, c was the specific heat, ρ was the density. The summation of inherent strain was calculated in Eq. (19) and (20), then inherent strain computation was loaded in the Eq. (23) and (24) respectively. A was the area of the element that the inherent strain was loaded.

$$\varepsilon_x^* = W_x/A \quad (23)$$

$$\varepsilon_y^* = W_y/A \quad (24)$$

Determination of effective area

The modeling of the user-defined distortion with inherent strains method welding simulation combines the effect of plastic strains, thermal strains and phase transformation strains as structural boundary conditions. The area subjected to high temperature during the welding process is the effective area and location of the inherent strain to be determined. The welding performed at the same place with a different welding heat input, the inherent strain distribution was decided by the larger welding heat input, and the longitudinal shrinkage after three-pass welding.^[4] The structural analysis was setup with the weld path and filler. Based on the above equations the coefficient K and ξ of longitudinal inherent strain (ε_x^*) and the transverse inherent strain (ε_y^*) as the boundary conditions for each layer is calculated for first, second and third weld layer respectively (computed values of ε_x^* : 0.0142, 0.0121 and 0.0012; and ε_y^* values: 0.0473, 0.0305, 0.0301). The values were assigned for all elements of the effective area observed, calibrated front view illustrated in Fig. 2(c). the thermal expansion coefficient α , specific heat capacity C_p , and mass density ρ were $1.2 \times 10^{-5} \text{ K}^{-1}$, $0.46 \text{ Jg}^{-1} \text{ K}^{-1}$ and $7.850 \times 10^{-3} \text{ g.mm}^{-3}$, respectively.

Experimental welding procedure

Robotic welding ABB IRB 2400/16 with GMAW power source KEMMPI ProEvolution ProMIG 540 MXE welding torch movement with ER80s-Ni1 filler wire of 1.2 mm diameter for the filler welds in three passes weld deformation behavior of the 10 mm thickness HSLA steel S460 10 mm was investigated without pre-heat due to partial refined grain, recrystallization and probably second phase constituent part, therefore the existing WPS and PQR cannot be relied on.^[30] Prior to welding, each pass of welding variables was optimized for sound welds with welding procedure specification (WPS) generated according to the welding practice of AWS D1.1 and verified in-house with 100 mm length and 150 mm width plate. All three passes used mixed shielding gases. 80% Ar + 20% CO₂% was selected based on the guidelines as stipulated in AWS A5.28:2005 with moderation achieved with a gas flow meter with 16–18 L/min on the 10 mm thickness welded plates with V-groove weld joint design.

Subsequently, Macro Etching was performed to reveal the fusion line (boundary) between weld metal and base metal to determine the soundness of a weld. Furthermore, the contour

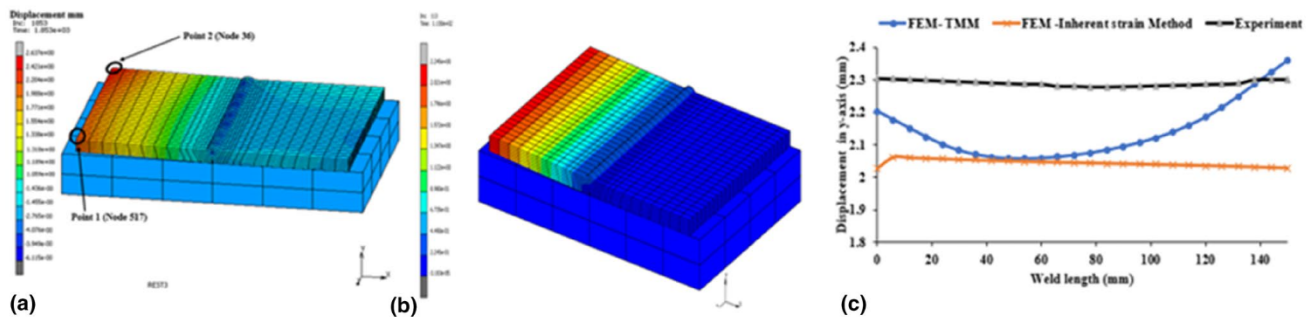


Figure 3. Angular distortion prediction by length (a) TMM (thermal elastic simulation) (b) ISM (elastic simulation) and (c) comparison distortion result of welding simulation and experiment.

of the plate top at the unclamped section was measured with Mitutoyo coordinate measuring machine (CMM), and the 3D-Geopak-3 CNC v5.21 software was used to characterize the data point measured by CMM. The sensor tip was placed at the surface of the table bar of the CMM to create the datum coordinate set before measuring the top part of the welded specimen which was subtracted from the plate thickness earlier measured as depicted in.

Result and discussions

The simulated results for predicting weld deformations of the multi-pass welding joint were compared with the experiment. For the solver, a direct solver was used to run the solid mechanic computation with a multi-frontal parallel sparse algorithm. Also, the software-running environment was the 64-bit windows 10 system with a 32-GB RAM, CPU 3.20 GHz, and core-i7 processors, and the total analysis time was 113 s for ISM-UD model. However, thermo-mechanical FEM computation with 4 solver threads had an analysis time of 1853 s.

Distortion

The transverse and longitudinal inherent strains of the butt-joint were obtained based on empirical formulas by inherent strain method for each layer. Consequently, based on the calculation results of the empirical formula of inherent strain method. Predicted results demonstrate the weld deformation caused by the three-layer gas metal arc welding. Comparison of distortion result along weld length produced by FEM thermo-mechanical and inherent strain methods as shown in the model plot in Fig. 3(a, b). After cool-off, distortion measurements of the welding experiment along the same point with the simulations results is depicted in Fig. 3(c). Mochizuki M. et al. and Mato Peric et al. results display a similar trend of vertical displacement between the methods of thermal-elastic-plastic analysis and elastic prediction.^[31, 32] Several reasons may have accounted for the peak differences between the predicted TMM and measured distortion is 2.358% error while 11.7% error was observed in the case of ISM -UD. The calibration of the effective area was ensured. However, the FE weld simulation

assumptions discussed above and errors in the other measurements might produce uncertainty in the magnitude of the measured distortion. The experimental result of two endpoints was selected as a tracking point for measurement in which the average value through these points value serves as a benchmark of comparison.

Conclusion

The effectiveness of the inherent strain method for elastic FEM in distortion prediction in GMAW simulation process of HSLA steels is studied to improve the quality and to reduce the time and cost of welding deformation process developments. The obtained results are summarized as follows:

1. The numerical analysis of weld distortion of butt-joint can be calculated in reasonable computing time with less load case using the inherent strain method
2. Compared to thermo-mechanical simulation, the simplified inherent strain model allows processing and computational time to be reduced by about 93.9%.
3. The thermal calibration analysis was conducted which shows the similarities of the temperature distribution pattern between welding simulation and experiment for the thermo-mechanical FEM.
4. The predicted welding distortion TMM results display the error percentage within the range of 1–5.3% in comparison with the experiment, however, that of inherent strain method was about 6–9% range. Due to its accuracy and efficiency, the ISM will be able to substitute TMM analysis which requires much more computing time.

Acknowledgments

The authors would like to express their gratitude to staff member of Smart Manufacturing Research Institute (SMRI) as well as the staff of Advanced Manufacturing Laboratory, at Faculty

of Mechanical Engineering, Universiti Teknologi MARA (UiTM) Malaysia, as well as Tertiary Education Trust Fund (TETFund) and University of Ilorin, Nigeria for the TETF/ES/UNI/ILORIN/ASTD/2018 intervention.

Declarations

Conflict of interest

The authors declare that no competing interests exist.

References

1. R.C. Cochrane, Phase transformations in microalloyed high strength low alloy (HSLA) steels, in *Phase Transformations in Steels*, 1st edn., ed. by E. Pereloma, D. Edmonds (Woodhead Publishing Limited, Sawston, 2012), pp. 153–212
2. H.K.D.H. Bhadeshia, R. Honeycombe, *Steels: Microstructure and Properties*, 3rd edn. (Butterworth-Heinemann, Oxford, 2006)
3. J. Hensel, T. Nitschke-Pagel, D. Tchoffo Ngoula, H.T. Beier, D. Tchuindjang, U. Zerbst, Welding residual stresses as needed for the prediction of fatigue crack propagation and fatigue strength. *Eng. Fract. Mech.* **198**, 123–141 (2018)
4. T. Terasaki, T. Fukikawa, T. Kitamura, T. Akiyama, Welding deformation produced by two-pass welding. *Weld. Int.* **23**(11), 830–838 (2009)
5. Y. Lu, C. Lu, D. Zhang, T. Chen, J. Zeng, P. Wu, Numerical computation methods of welding deformation and their application in bogie frame for high-speed trains. *J. Manuf. Process.* **38**, 204–213 (2019)
6. L.E. Lindgren, J. Edberg, P. Åkerström, Z. Zhang, Modeling of thermal stresses in low alloy steels. *J. Therm. Stresses* **42**(6), 725–743 (2019)
7. D. Deng, H. Murakawa, W. Liang, Numerical simulation of welding distortion in large structures. *Comput. Methods Appl. Mech. Eng.* **196**(45–48), 4613–4627 (2007)
8. H. Murakawa, S. Rashed, S. Shinji, Prediction of distortion produced on welded structures during assembly using inherent deformation and interface element. *Trans. Japan Weld. Res. Inst.* **38**(2), 63–69 (2009)
9. D. Deng, H. Murakawa, Prediction of welding distortion and residual stress in a thin plate butt-welded joint. *Comput. Mater. Sci.* **43**(2), 353–365 (2008)
10. Y. Kim, J. Kim, and S. Kang, 'A study on welding deformation prediction for ship blocks using the equivalent strain method based on inherent strain', *Applied Sciences (Switzerland)*, vol. 9, no. 22, 2019.
11. Y. Luo, H. Murakawa, Y. Ueda, Prediction of welding deformation and residual stress by elastic FEM based on inherent strain (Report I): mechanism of inherent strain production (Mechanics, Strength & Structure Design). *Trans. JWRI* **26**(2), 49–57 (1997)
12. C.D. Jang, Y.T. Kim, Y.C. Jo, H.S. Ryu, Welding distortion analysis of hull blocks using equivalent load method based on inherent strain. *10th International Symposium on Practical Design of Ships and other Floating Structures, PRADS 2007*, vol. 2, pp. 889–893 (2007).
13. Y. Ha, J. Choi, Cumulative angular distortion curve of multi-pass welding at thick plate of offshore structures. *J. Adv. Res. Ocean Eng.* **1**(2), 106–114 (2015)
14. S. Okano, S. Tadano, Y. Nakatani, M. Mochizuki, Assembling a database of inherent strain for simplified distortion analysis in multi-layer and multi-pass welding of heavy section plate (Development of accuracy management system for high quality construction in welded structures on the basis of advanced. *Trans. JSME*, pp. 16-00005 (2016).
15. T. Satoshi, M. Rieko, S. Kouji, N. Yuijiro, Experimental and numerical study of welding deformation in truss structure of steel angles. J-stage 溶接学会論文集 **37**(1), 52–58 (2019)
16. MSC Software, 'Volume A: Theory and user information', 2019.
17. M. S. Davoud and X. Deng, 'Finite element modeling of GMAW process: Evolution and formation of residual stresses upon cooling', in *ASME International Mechanical Engineering Congress and Exposition*, 2004, pp. 1–7.
18. J. G. Mullins and J. Gunnars, 'Effect of hardening model on the weld residual stress field in pipe girth welds', *International Conference on Structural Mechanics in Reactor Technology*, no. SMiRT 20, pp. 1–10, 2009.
19. U. Diekmann, 'Calculation of steel data using JMatPro', in *Comat 2012: Recent trends in structural materials*, 2012, p. 6.
20. N. Saunders, Z. Guo, X. Li, A.P. Miodownik, J.P. Schillé, Using JMatPro to model materials properties and behavior. *JOM* **55**(12), 60–65 (2003)
21. J.A. Goldak, M. Akhlaghi, *Computational Welding Mechanics* (Springer, New York, 2005)
22. D. Deng, Y. Zhou, T. Bi, X. Liu, Experimental and numerical investigations of welding distortion induced by CO₂ gas arc welding in thin-plate bead-on joints. *Mater. Des.* **52**, 720–729 (2013)
23. N. Ma et al., Inherent strain method for residual stress measurement and welding distortion prediction. *International Conference on Offshore Mechanics and Arctic Engineering* (Vol. 50008, p. V009T13A001). American Society of Mechanical Engineers.
24. T.J. Kim, B.S. Jang, S.W. Kang, Welding deformation analysis based on improved equivalent strain method considering the effect of temperature gradients. *Int. J. Naval Archit. Ocean Eng.* **7**(1), 157–173 (2015)
25. Y.X. Wang, P. Zhang, Z.G. Hou, C.Z. Li, Inherent strain method and thermal elastic-plastic analysis of welding deformation of a thin-wall beam. *J. Mech.* **24**(4), 301–309 (2008)
26. Y. Ueda, H. Murakawa, N. Ma, Simulation Procedures for Welding Heat Conduction, Welding Deformation, and Residual Stresses Using the FEM Programs Provided on the Companion Website. in *Welding Deformation and Residual Stress Prevention*, Elsevier, 2012, pp. 169–207.
27. C. Jun-mei, L. U. Hao, W. Jian-hua, C. Wei-xin, and H. Da-Jun, in Prediction of Welding Deformation With Inherent Strain Method Based on FEM, *ANSYS Support*.
28. C.D. Jang, S.I. Seo, A study on the prediction of deformations of plates due to line heating using a simplified thermal elasto-plastic analysis. *J. Soc. Naval Archit. Korea* **34**(3), 104–112 (1997)
29. T.J. Kim, B.S. Jang, S.W. Kang, Welding deformation analysis based on improved equivalent strain method to cover external constraint during cooling stage. *Int. J. Naval Archit. Ocean Eng.* **7**(5), 805–816 (2015)
30. M.M. Hosseinioun, G. Moeini, C. Konke, A. Tahaei, Investigations on multi-run metal made of HSLA steel—heterogeneous microstructure and mechanical properties. *Mater. Test.* **59**(7–8), 661–672 (2017)
31. M. Mochizuki, Y. Mikami, H. Yamasaki, M. Toyoda, Elastic predicting method of weld distortion of large structures using numerical simulation results by thermal-elastic-plastic analysis of small components. *Weld. World* **51**(11–12), 60–64 (2007)
32. M. Perić, K. Seleš, Z. Tonković, M. Lovrenić-Jugović, Numerical simulation of welding distortions in large structures with a simplified engineering approach. *Open Phys.* **17**(1), 719–730 (2019)